A 915 MHz 175 μW Receiver Using Transmitted-Reference and Shifted Limiters for 50 dB In-Band Interference Tolerance

Dawei Ye, Ronan van der Zee, Bram Nauta,

University of Twente, IC Design Group, CTIT Institute, Enschede, The Netherlands

Contact Information:

Name: Dawei Ye

Address: University of Twente, Carre 2724, P.O Box 217, 7500 AE Enschede, The Netherlands,

Phone: +31 53489 5207, Fax: +31 53 4879 1034, E-mail: d.ye@utwente.nl

Abstract – Improving interference robustness in Ultra-Low Power (ULP) receivers is a big challenge due to their low power budget. This paper presents an envelope detector based 915MHz 10kbps ULP receiver, which is fabricated in 65nm CMOS process for Wireless Sensor Networks (WSN) and Internet of Things (IoT). Two power-efficient techniques: Transmitted-Reference and Shifted Limiter, are proposed to improve the interference robustness. The receiver sensitivity is between -61 and -76dBm. The maximum in-band Signal-to-Interference Ratio (SIR) at +/-1MHz offset is up to -50dB while just consuming 175μW power from a 1V supply.

Keywords –wireless sensor network, internet of things, RF, transmitted-reference, shifted limiter, CMOS, ULP receiver, envelope detector, interference robustness, spread-spectrum, fast synchronization, LNA, linear range, gain compression, probability density function, SIR.

I. Introduction

Ultra-Low Power (ULP) radios have received a lot of attention recently, especially for short-range low-data rate applications in Wireless Sensor Networks (WSN) and Internet-of-Things (IoT). However, for radios to coexist with the many wireless standards in the ISM bands (Bluetooth, WLAN, ZigBee etc.), interference robustness of ULP receivers (RX) is a challenge in the limited power budget (~100µW) [1]. Several works [2-9] have been published recently for the implementation of ULP receivers. Reference [2] proposes a superheterodyne receiver combined with a low power Local Oscillators (LO). However, the LO requires an external inductor to achieve good phase noise to avoid reciprocal mixing at low power, while non-linearity and limited RF filtering make it vulnerable to in-band interferers. To reduce the number of external components, Envelope Detector (ED) based receivers are proposed [3-7]. However, their selectivity and linearity are poor if an external high-Q filter is not used. By sending two narrow band signals which are spaced by a small frequency offset to the ED based receiver [8], the problem can be partially solved. This is because after the ED, the intermodulation product from the two signals will locate at the frequency offset instead of DC and will not overlap with the interferers except for some specific interferer frequencies. However, to obtain good sensitivity in such envelope detector based receivers, high gain Low Noise Amplifiers (LNA) are needed. Since these LNAs process the entire frequency band, strong in-band interferers will quickly saturate these LNAs, compressing the signal gain [4-8]. To break the trade-off between power, sensitivity and linearity, while improving the interference robustness, we propose an ULP receiver that uses two techniques: Transmitted-Reference (TR) modulation and Shifted Limiters (SL) [9]. Compared to [9], theoretical background is added in this paper, as well as circuit details and new measurements are given.

The rest part of the paper is structured as follows: Section II illustrates the basic concepts and principles of TR and SL. Section III explains the circuit details of the proposed RX and the corresponding measurement results are included in Section IV. Finally, the conclusions are drawn in Section V.

II. Improving interference robustness

This section presents the two main concepts that allow the interference robustness of the receiver: transmitted reference (subsection A) and shifted limiters (subsection B). The latter needs envelope tracking, which is discussed in subsection C.

A. Transmitted-Reference Modulation

Unlike narrow band modulation, Spread-Spectrum (SS) modulation [10] can cope better with narrow interferers and fading dips in the channel due to its frequency independent selectivity and wide band transmission. However, in the receiver the spread sequence has to be locally generated as a reference to synchronize the received signal which will take extra time [11], preventing the extreme duty-cycling common in WSNs. To shorten the synchronization time, Transmitted-Reference (TR) [12] modulation is proposed, as shown in figure 1. The TX output consists of the (upconverted) addition of two signals: a spread sequence, and that same sequence which is modulated and shifted in frequency by $\Delta\omega$. The output signal from this transmitter can thus be written as

$$V_{TXout}(t) = m(t)D(t)\cos(\omega_{sig}t)\cdot\cos(\Delta\omega t) + m(t)\cos(\omega_{sig}t) \quad (1)$$

where $m(t)$ is a pseudo random (PN) sequence for SS modulation, randomly switching between 1 and -1, satisfying $m^2(t) = 1$. $D(t)$ is the desired data, ω_{sig} is the carrier

frequency, Δω is a small frequency offset ($\ll \omega_{RF}/100$). The phase of the TX signal is irrelevant, as it will be auto-correlated in the receiver. The main difference with typical spread spectrum is that the spread reference sequence is not generated in the receiver but included in the output signal of the transmitter, shifted by Δω. If we neglect the propagation loss and noise from the wireless channel, the RX input signal $V_{RXin}(t)$ equals $V_{TXout}(t)$, and the spectrum is displayed in the left of Fig. 2(a). Then after the x^2 Envelope Detector (ED), the signal $V_{SQout}(t)$ is given by

$$V_{SQout}(t) = \frac{1}{4}D^2(t)(1+\cos 2\omega_{sig}t)(1+\cos 2\Delta\omega t) + \frac{1}{2}(1+\cos 2\omega_{sig}t) + D(t)(1+\cos 2\omega_{sig}t)\cos\Delta\omega t \quad (2)$$

A practical ED will also contain higher order terms, but we focus on the term around Δω, which equals $D(t)\cos\Delta\omega t$. By mixing everything down to $(\Delta\omega - \omega_{IF})$ and filtering it by the baseband filter, the output signal $V_{IFout}(t)$ is given by:

$$V_{IFout}(t) = \frac{1}{2}D(t)\cos(\Delta\omega - \omega_{IF})t \quad (3)$$

where $\omega_{IF}(<\Delta\omega)$ is the frequency of the LO at the intermediate stage. $V_{IFout}(t)$ is then demodulated in the baseband processor. Now, when an interferer falls into the band of interest, the RX input signal changes to,

$$V_{RXin}(t) = m(t)D(t)\cos\omega_{sig}t \cdot \cos\Delta\omega t + m(t)\cos\omega_{sig}t + V_{int}(t)\cos\omega_{int}t \quad (4)$$

where $V_{int}(t)$ is the interferer amplitude and ω_{int} is the frequency of interferer. Then, the output signal of the intermediate stage is derived as (neglecting the frequency terms which can be rejected by the band-pass filter at $(\Delta\omega - \omega_{IF})$:

$$V_{IFout}(t) = \frac{1}{2}D(t)\cos(\Delta\omega - \omega_{IF})t + m(t)V_{int}(t)\cos(\omega_{int} - \omega_{sig})t \cdot \cos\omega_{IF}t \cdot [D(t)\cos\Delta\omega t + 1] \quad (5)$$

The corresponding illustration in the frequency domain is shown in figure 2(b). $m(t)$ spreads out the interferer to a wider frequency range, so most of the undesired power is rejected by the band-pass filter, improving the Signal-to-Interference-Ratio (SIR). When multiple interferers fall into the interested band, the TR modulation will become less effective because after ED, the non-spread intermodulation tones between these interferers could be very close to $\Delta\omega$. In the worst case, if the frequency distance of two interferers equals exactly $\Delta\omega$, their intermodulation product will be located at $\Delta\omega$, severely degrading the SIR. The m(t) bandwidth is chosen based on the knowledge that a wider spreading bandwidth can enhance the interference robustness. However, the maximum spreading bandwidth is limited by the available spectrum and the power budget of the system. Regarding the choice of $\Delta\omega$, a higher $\Delta\omega$ will make the down-converted signal less sensitive to flicker noise. The maximum $\Delta\omega$ is limited both by the available spectrum and by the coherence bandwidth of the channel (the two frequency-shifted bands should see the same channel in order to have sufficient correlation for demodulation).

In summary, TR modulation has three advantages: a) Compared to narrow band modulation, it provides frequency independent selectivity to suppress in-band interferers and is more robust to fading dips in the wireless channel. b) Unlike general SS, since the synchronized reference is included in the received signal the synchronization can be instantaneous by using an ED. Hence no start-up time is needed for synchronization of the spreading sequence. c) Due to the frequency offset $\Delta\omega$ in the received signal, the desired data is not down-converted to DC but to $\Delta\omega$ (figure 2). This can help to reduce the influence of DC offset and flicker noise.

B. Shifted Limiters

Since an ED is used to replace the LO for frequency down-conversion, an LNA with considerable voltage gain (>40dB) is needed to obtain a decent Noise Figure (NF) [4-8]. This is common in ED based receivers, but it has the drawback that when a strong interferer is present, it will move the RX chain into compression and reduce the wanted signal gain. We take a strong interferer + wanted signal as the input

$$V_{IN} = V_{int} \sin \omega_{int} t + V_{sig} \sin \omega_{sig} t \ , \ \ V_{sig} \ll V_{int} \tag{6}$$

where V_{int} and V_{sig} represent the interferer and desired signal amplitudes respectively, and the interferer frequency ω_{int} is close to the signal frequency ω_{sig}. The LNA can roughly be modelled as a constant linear gain G_S with clipping points V_{TH} and V_{clip}, assuming the gain is 0 below V_{TH} and above V_{clip} as shown in Figure 3. Then the transfer function can be defined as:

$$v_{OUT} = f(v_{IN}) = \begin{cases} VDD & , v_{IN} \geq V_{clip} \\ G_S \cdot (v_{IN} - V_{TH}) & , V_{TH} < v_{IN} < V_{clip} \\ 0 & , v_{IN} \leq V_{TH} \end{cases} \tag{7}$$

Then the conversion gains of interferer and signal are derived as (see Appendix A)

$$G_{int} = \frac{1}{\pi V_{int}} \int_{-\pi}^{\pi} f(V_{int} \sin \theta_2) \sin \theta_2 \, d\theta_2 \tag{8}$$

$$G_{sig} = G_S \cdot \int_{V_{TH}}^{V_{clip}} PDF_{sin}(x) \, dx \tag{9}$$

where $PDF_{sin} = 1/(\pi \sqrt{V_{int}^2 - x^2})$ for $-V_{int} < x < V_{int}$ and $= 0$ for others, is the Probability Density Function of a sinusoidal wave. (8) shows that if $V_{sig} \ll V_{int}$, G_{int} can be approximated as the ratio between the fundamental tone of the interferer output and its input counterpart. The physical meaning of (9) is that since the biasing point x of the LNA is varied by the sinusoidal amplitude of the interferer ($V_{int} \sin \omega_{int} t$), the effective small signal

gain of the LNA will be the normal small signal gain, weighted by the amplitude probability density of the interferer. Hence, if the amplitude PDF of the interferer is known, G_{sig} can be calculated by (9).

The above analysis is visualized in Figure 4(a) which shows the PDF_{sin} of V_{int} when the linear region of the LNA is centred around the middle of V_{int} . It can be seen that since most of the signal power is presented in the interferer peaks, the low value of PDF_{sin} will cause deterioration of G_{sig}. To avoid this compression, the typical method is to widen the linear range to cover the full PDF_{sin}, but this will increase the power consumption. In our case, instead of increasing the linear range, we move it to one of the interferer peaks (figure 4(b)). Then the PDF_{sin} within the linear range becomes higher, relaxing the compression of G_{sig}. In contrast to extending the linear range, the proposed idea doesn't consume much extra power since the linear range in (7) is not increased but just shifted by $V_{int}(V_{TH} = V_{int})$, as shown in figure 5. Moreover, after moving the linear range, only the lower part of v_{OUT} is clipped while its upper part is away from V_{DD} and hence can be amplified. Because of this shifting of the linear range, we call this technique a Shifted Limiter (SL). The concept of this technique was first proposed in [13], and it will introduce considerable intermodulation between the frequency components of the input signal. Although this partly contributes to the TR demodulation, it can also degrade the system performance in specific situations, as we will see with the SIR measurements in section IV.

By using (7), (8) and (9), we can theoretically analyse the influence of G_S, V_{clip} and V_{TH} on G_{sig}, G_{int} and G_{sig}/G_S, as shown in figure 6. Figure 6(a) shows the normalized conversion gains G_{sig}/G_S (G_{int}/G_S) as a function of V_{int} in a (non-shifted) limiter. As long as $V_{int} < V_{clip}$, G_{sig} and G_{int} are constant and equal. When $V_{int} > V_{clip}$, both G_{sig} and G_{int} are compressed. However, the reduction of G_{sig} is faster than the reduction of G_{int}, degrading the

SIR. On the other hand, if the middle of the linear range moves to V_{int} , the limiter is changed to a shifted limiter (figure 6(b)). Then, within the linear range $[V_{TH}, V_{clip}]$, G_{sig} becomes larger than G_{int}, improving the SIR. It is also interesting to investigate the relationship between the SIR improvement (G_{sig}/G_{int}) and V_{TH} in the SL. As shown in figure 6(c), when V_{TH} is changed from V_{TH1} to V_{TH2} ($V_{TH2} = 2V_{TH1}$) the G_{sig}/G_{int} at V_{clip} is improved from 7.8dB to 11.9dB while the related maximum G_{sig} is reduced. Since V_{TH} has to be adjusted to ensure that V_{int} is always in the middle of the linear range, the SL will have better SIR improvement for a higher V_{int} at the expense of G_{sig}. The SIR improvement for different V_{TH} is shown in figure 6(d). On the other hand, if G_S is reduced from 26 to 20dB, as shown in figure 6(e), G_{sig} and G_{sig}/G_{int} (at V_{clip}) will be accordingly decreased by 6 and 3dB, respectively. Hence we can conclude that by using the SL, a higher G_S can further improve the SIR and G_{sig}. This is completely different from techniques that rely on linearization to be interferer robust [14-15], which require a small G_S.

C. SL for interferers with variant envelopes

The above analysis is based on the assumption that V_{int} = constant. However, when V_{int} is not constant the SL would be less effective due to the fact that the PDF of V_{int} becomes unknown. To cope with a varying V_{int}, an Envelope Tracking and Adjusting (ETA) block is needed, which can reshape the V_{int} to a constant envelope before the interferer reaches the SL. Figure 7(a) shows the principle of the ETA in time domain. The ETA removes the variation in V_{int} and hence changes the unknown PDF of V_{int} to PDF_{sin}, which can be handled by the SL. Figure 7(b) illustrates the principle of the ETA in the frequency domain. The variation of V_{int} is regarded as an interferer sideband (Interf.2) around its fundamental tone (Interf.1) and the distance between them is BW_{int}. Further, the distance between the

Interf.1 and signal is f_{SI}. The ETA is equivalent to an Auto-Gain-Control (AGC) block, whose specific target is to remove the Interf.2 while keeping the signal and Interf.1 unchanged. This can be achieved if the bandwidth of the ETA (BW_{ETA}) meets

$$BW_{int} < BW_{ETA} < f_{SI} \tag{10}$$

Then, after the ETA, Interf.2 is greatly attenuated, resulting in an interferer with constant V_{int} which can be suppressed by the SL.

III. Implementation of the proposed receiver

A. Shifted limiter

There are many possible ways to implement the SL. One implementation is shown in figure 8(a), which is simply a differential pair with current mirror load. We assume V_{sig} is very small and can be neglected, v_{IN} is the input signal with amplitude $\approx V_{int}$, V_D is the output biasing voltage for zero differential input to the differential pair and v_{OUT} is the total output signal. v_{IN} is applied to the gate of M_1 and a DC voltage V_P is applied to the gate of M_2. Figure 8(b) shows the simulated DC characteristics. When V_P is 500mV, the transfer function (red) with respect to v_{IN} has a linear range which is limited by V_{-CLIP} and V_{CLIP} and its slope is assumed to be a constant $-G_S$. When V_P is increased by V_{int} (= 0.1V, for instance), the linear range of the differential pair is shifted away from v_{IN} = 500mV, realizing the SL. Hence the large signal transfer function of the proposed SL can be ideally defined as

$$v_{OUT} = \begin{cases} V_S & , v_{IN} \geq V_{CLIP} \\ V_{DD} - G_S \cdot (v_{IN} - V_P) & , V_{-CLIP} < v_{IN} < V_{CLIP} \\ V_{DD} & , v_{IN} \leq V_{-CLIP} \end{cases} \tag{11}$$

Compared to (7), (11) has an inverse slope polarity of the linear range and different DC levels of the clipping range. Furthermore, in contrast with the initial transfer function (red), the

shifted one (blue) has a smaller linear range due to the fact that the increment of V_P ($= \Delta V_P$) will increase V_S ($= \Delta V_S$). Next, we would like to estimate the maximum output range of the SL. Since for a SL, $\Delta V_P = V_{int}$, by considering (11) and figure 8, the peak-to-peak value of v_{OUT} will be:

$$V_{OUT\_PP} = V_{DD} - V_D \tag{12}$$

(12) defines the amplitude of the interferer at the output of the proposed SL. It is clear that a higher V_D can decrease the interferer amplitude. Also, the linear part between V_D and V_S is not used for amplification if ΔV_P is exactly the same as V_{int}. Figure 8(c) shows the relationship between simulated normalized conversion gains ($\Delta V_P = 0.1$V) and V_{int}. As we see, if $\Delta V_P = V_{int}$, the SIR will be improved. This result well matches the theoretic analysis in figure 6(b). On the other hand, (12) is valid only when $\Delta V_P = V_{int}$. In practical design, it is difficult to exactly obtain the envelope information of a large signal. For example, if the mismatch between ΔV_P and V_{int} is δV_{int}, then (12) will be changed to

$$V_{OUT\_PP} = V_{DD} - V_D + G_S \delta V_{int} \tag{13}$$

Suppose $\delta = 10\%$, $G_S = 26$dB and $V_{int} = 0.1$V, the maximum output signal will be increased by 0.2V. Then for a 1V V_{DD}, the subsequent stage has to increase or shift its linear range by more than 20% to cope with this 10% mismatch. In the worst case, if $G_S \delta V_{int}$ is higher than $V_D - V_S$, the transfer function with respect to v_{IN} will become a typical limiter which will degrade the SIR. To obtain an accurate ΔV_P, one possible solution is a feedforward control path [16], but this uses too much power. In this work, we design a feedback control loop (figure 9(a)), which consists of a SL and an envelope tracker. The envelope tracker is composed of an active diode M_6 which works in weak inversion and a capacitor C_P filtering out the RF signal such that only the positive envelope of v_{IN} remains. The functionality of the SL can be realized if the closed-loop gain for the input envelope ($G_{CL} = \Delta V_P / V_{int}$) is close to

1, then ΔV_P will equal V_{int}, shifting the middle of the linear range of the differential pair to the positive interferer peaks. By tuning the biasing current I_{BET}, g_{m6} (the transconductance of M_6) can be set to adjust the bandwidth of the ETA loop (BW_{ETA}) . To derive G_{CL}, we first know that the gate-source input voltage of M_6 (v_{IN6}) is (neglecting the small signal $V_{sig}\sin\omega_{sig}t$)

$$v_{IN6} = V_{DD} - V_D - G_S(G_{CL}V_{int} - V_{int}\sin\omega_{int}t) \tag{14}$$

Then i_{OUT6} is represented as

$$i_{OUT6} = I_0\frac{W}{L}\exp\left(\frac{v_{IN6}}{nV_T}\right) = I_0\frac{W}{L}\exp(\frac{VDD-V_D}{nV_T})\exp(\frac{-G_SG_{CL}V_{int}}{nV_T})\exp(\frac{G_SV_{int}\sin\omega_{int}t}{nV_T}) \tag{15}$$

Where I_0 is a process dependent current and W and L are the width and length of M_6 respectively. $n = 1.5$ for weak inversion and $V_T = 26\text{mV}$ at 300K. We assume a sinusoidal v_{IN6} here, although the actual waveform (see Figure 8a) is clipped. However, since i_{OUT6} is an exponential function with respect to v_{IN6}, the contribution from the upper half of v_{IN6} to i_{OUT6} is negligible, so we can still use this assumption. The term $\exp(G_SV_{int}\sin\omega_{int}t/nV_T)$ in (15) can be expanded to a Fourier series

$$i_{OUT6} = I_t\exp\left(\frac{-G_SG_{CL}V_{int}}{nV_T}\right)\cdot\left(J_0\left(\frac{G_SV_{int}}{nV_T}\right) + \sum_{k=1}^{\infty}2J_k\left(\frac{G_SV_{int}}{nV_T}\right)\cdot\cos k\omega_{int}t\right) \tag{16}$$

where $I_t = I_0(W/L)\exp((V_{DD}-V_D)/nV_T)$ and J_n is the n^{th} order modified Bessel function of the first kind. Due to C_P, the high order frequency components ($k \geq 1$) can be neglected. Hence (16) is approximated as

$$i_{OUT6} \approx I_t\exp\left(\frac{-G_SG_{CL}V_{int}}{nV_T}\right)J_0(\frac{G_SV_{int}}{nV_T}) \tag{17}$$

If $G_SV_{int}/nV_T \geq 2$, (17) can be approximated as [17]:

$$i_{OUT6} \approx I_t\exp\left(\frac{G_SV_{int}-G_SG_{CL}V_{int}}{nV_T}\right)\sqrt{\frac{nV_T}{2\pi G_SV_{int}}} \tag{18}$$

Since i_{OUT6} only contains the DC term, the loop will force it to be equal to the bias current I_{BET}, so G_{CL} can be written as

$$G_{CL} = 1 - \frac{nV_T}{G_S V_{int}} \cdot \ln\left(\frac{I_{BET}}{I_t}\sqrt{2\pi\frac{G_S V_{int}}{nV_T}}\right) \quad (19)$$

Figure 9(b) shows the comparison between the simulated and calculated G_{CL} for different V_{int} and the error is less than 5%. The deviation at low amplitudes is not a problem since the differential pair has sufficient linear range to handle the difference. With (13) and (19), we can now calculate the output interferer level

$$V_{OUT\_PP} = V_{DD} - V_D + G_S V_{int} \cdot (1 - G_{CL}) = nV_T \cdot \ln\left(\frac{L}{W}\frac{I_{BET}}{I_0}\sqrt{\frac{2\pi G_S V_{int}}{nV_T}}\right) \quad (20)$$

(20) indicates that for a certain interferer amplitude V_{int}, the proposed SL (figure 9(b)) can improve the interference suppression by decreasing I_{BET} or G_S. However, decreasing I_{BET} will reduce the BW_{ETA} which will determine the performance of the SL for AM interferers. Similarly, G_{sig} is proportional to G_S (figure 6(e)) and a large G_{sig} is necessary for good sensitivity [5]. Therefore, a trade-off between G_S and BW_{ETA} should be carefully considered. Moreover, combining (9), and (20), we can estimate the SIR improvement by:

$$\frac{G_{sig}}{G_{int}} = \frac{2V_{int}G_S \cdot \int_{V_{-CLIP}}^{V_{CLIP}} PDF_{sin}(x)dx}{\alpha nV_T \cdot \ln\left(\frac{L}{W}\frac{I_{BET}}{I_0}\sqrt{\frac{2\pi G_S V_{int}}{nV_T}}\right)} \quad (21)$$

where α is the ratio between the fundamental and total power of the output interferer.

B. Proposed receiver architecture

Figure 10 shows the proposed RX front-end combing the TR and SL techniques. The SL is slightly different from figure 9(a); the differential-pair LNA is cascoded to reduce its output capacitance for maintaining the voltage gain at RF frequency. Multiple SLs are introduced to further improve the SIR in the presence of a large interferer. When the interferer is weak,

single-ended linear LNAs with an active inductance load can replace the SL to save power. Before the down-conversion, three RF paths (1-3) with different numbers of linear LNAs and SLs are realized on the same chip and can be selected for different interferer levels. Further, an input matching network with an external SMD inductor provides ≈ 12dB passive voltage gain. The small signal gain (G_S) of each linear LNA/SL is ≈ 10dB and each RF path contains four LNA/SL stages, which provides ≈ 40dB G_S. Without an interferer, the simulated NF of the RF paths (from before the input matching network to before the ED) is around 12dB. When an interferer is added, RF path 2 and 3 will reduce G_{sig} as shown in figure 6 and the NF will increase, the magnitude depending on V_{int} and G_S. For example, when RF path 3 handles a -16dBm in-band interferer at 5MHz offset, the simulated NF degrades to 22dB. Additionally, the ED contributes to the overall NF, and due to its self-mixing this contribution depends on the absolute signal level [5]. The RF path is followed by an envelope detector and a selection switch. The envelope detector shown in [5] is adopted in this work; it works in weak inversion, with an exponential V-I function. Compared to the ideal squarer, its high even order terms also contribute to frequency down-conversion, increasing the conversion gain. After the ED, the DC term is rejected by AC coupling and the signal is down-converted to ($\Delta\omega - \omega_{IF}$) by an IF mixer stage consisting of a transconductor and a current mode double balanced passive mixer, and then further amplified and filtered by a 1st order filter. The gain of the IF mixer + filter is around 40dB, and the filter has a programmable bandwidth (10 – 100kHz). Typically, ($\Delta\omega - \omega_{IF}$) is chosen very low compared to $\Delta\omega$, such that undesired products like $2\Delta\omega - \omega_{IF}$ (see Figure 2) are sufficiently attenuated. In our measurements, for example, we chose $\Delta\omega = \omega_{IF}$ = 2π*1MHz (zero IF), and the filter set at 10kHz bandwidth. Since the interferer has been greatly suppressed by the SLs and the processing gain of the TR (10·log(spread bandwidth/data rate) = 33dB in our case) before it is translated to the IF band, the phase noise performance of the IF clock is

practically insignificant. An external crystal oscillator (for accuracy), which is not included in this work, can be used as the IF LO. The power consumption of a 1MHz crystal clock can be as low as 10 μW [18].

The cascade of SLs in Path 2 and Path 3 in Figure 10 poses an extra challenge. The output of a single SL is clipped half of the time to V_{DD} (see Figure 8). A subsequent SL can only adapt its linear range to the positive side of the signal, which is the clipped part, containing no information. Therefore, the SL chains in path 2 and 3 are realized with alternatingly N-type and P-type SLs, as shown in Figure 11.

Logic for switching between the paths is not included in this work, but could be based on simple clip detectors, as explained in the next section.

IV. Measurement results

The proposed RX was fabricated in a 65nm CMOS process. The micrograph is shown in figure 12 and the active area is 0.225mm^2. The prototype is bonded to a 40-leads QFN package, which is mounted on a PCB for measurement.

To measure the SIR improvement of the SLs, a two-tone input is provided to the chip and Path 3 is selected as active path. An on-chip test buffer with ≈ 30dB attenuation after the final SL of path 3 is used to output the RF signal of the SL chain. The corresponding spectrums are shown in figure 13. The desired signal is -61dBm and located at 915MHz. The interferer is 45dB larger than the desired signal while the frequency distance between them is 5MHz. Then after the input matching network, SL chain and output buffer, the SIR of the SL chain is improved by 35dB. Meanwhile, a strong IM3 arises at the output spectrum. This is caused by the intermodulation between the signal and interferer [19]. Intuitively, such a

strong IM3 will deteriorate the SIR of the RX in case the interferer is very close to the signal. We will get back to this at the SIR measurements.

Figure 14 shows measured performance of a single SL (the 1st one in Path 3) for an AM interferer. The output power spectrum of this SL is obtained by using another on-chip test buffer (with ≈ 18dB attenuation). The related input power spectrum is shown in figure 14(a). The frequency distance (BW_{int}) between the fundamental tone (Interf.1) and sideband (Interf.2) of the interferer is 400kHz while the distance (f_{SI}) between the signal and Interf.1 is 3MHz. The levels of signal, interf.1 and interf.2 are -56, -16 and -46dBm respectively. In order to obtain a sinusoidal PDF, the BW_{ETA} has to meet (10). A narrow BW_{ETA} (BW_{ETA}<BW_{int}) will result in a spectral regrowth of the interferers, while a wide BW_{ETA} (BW_{ETA}>f_{SI}) will remove the desired signal which is then regarded as a sideband of Interf.1. Figure 14(b) shows the output spectrum of the SL for $I_{BET} = 5$nA. The SIR between the signal and Interf.1 is improved by 10dB. However, the SIR between the signal and interf.2 remains unchanged and some undesired IM products arise. To avoid this spectral regrowth, we increase I_{BET} to 50nA, the related output spectrum is shown in figure 14(c). Compared to figure 14(b), the IM products disappear except for two dominating IM3s, and the level difference between the Interf.2 and signal is ≈ 0. However, the SIR between the signal and Interf.1 is reduced by 5dB. This can be understood by (20), which shows that v_{OUT} (≈ level of Interf.1) is proportional to I_{BET}. Figure 14(d) shows the relationships between the conversion gain of the signal (G_{sig}), Interf.1 (G_{int1}), interf.2 (G_{int2}) and I_{BET}. Higher values of I_{BET} will widen BW_{ETA} and hence increase G_{int1} slowly and reduce G_{sig} and G_{int2} simultaneously. However, G_{int2} is reduced more rapidly than G_{sig}, which is due to the fact that the ETA loop is fast enough to track and reduce Interf.2 while it is too slow to decrease the signal significantly. Therefore, increasing BW_{ETA} (I_{BET}) can help to reduce the sidebands of an AM interferer. The price we have to pay for a wider BW_{ETA} is a worse SIR

improvement between the signal and Interf.1. Given the uncertainty of the exact interferer scenario, I_{BET} can be chosen as the result of a compromise between these metrics.

The SIR of the whole TR RX for different Paths (1/2/3) is measured and shown in figure 15. The TR signal is centred at 915MHz and generated by the testing equipment. The data rate of the BPSK data is 10kbps, the symbol rate of the spreading sequence $m(t)$ is 20Mbps and the frequency offset $\Delta\omega$ is $2\pi \times 1$MHz. The measured sensitivity varies between -76dBm for Path 1 (all LNA) and -61dBm for Path 3 (all SL) with power consumption between 135μW and 175μW from a 1V supply. Compared to Path 1, the sensitivity in Path 3 is reduced by 15dB. This is due to the fact that without the interferer, the desired signal is so small that the input amplitude of each SL in Path 3 is dominated by the wideband Gaussian noise from the prior stages. The Gaussian PDF of the noise power is highest around zero amplitude. The ETA, however, moves the linear range in the direction of the positive peak of the noise, compressing G_{sig}. The TR signal is combined with a sinusoidal interferer and then sent to the proposed RX. As shown in figure 15(a), the signal power is 3dB higher than its sensitivity and the interferer frequency is swept in the band of interest. At each interferer frequency, the SIR of the RX can be determined by increasing the interferer power until the BER become worse than 10^{-3}. The related measured result is shown in figure 15(b), the SIR for Path1/2/3 is -8/-26/-50dB, hence the advantage of the SLs can clearly be observed as the SIR is improved by 42dB from Path 1 to 3. The maximum tolerated interferer power of the RX is up to -8dBm, which is limited by the input window of the first SL and determines the maximum SIR. The SIR of the other paths is also limited by compression. This is because the envelope detector needs a rather strong signal to be effective, so there is very little headroom for an interferer. E.g. the simulated 1dB compression point of path 1 is -63dBm. This is very close to the measured sensitivity (-76dBm) + 3dB (used in the SIR measurement) + 8dB (measured 1/SIR) = -65dBm. Similarly for path 2, where the simulated 1dB compression point after the

2 LNA stages is -41dBm, which is close to the measured sensitivity (-70dBm) + 3dB + 27dB (measured 1/SIR) = -40dBm. As a consequence, as long as an interferer does not compress a path, the SIR in this path is always sufficient to get proper demodulation, and switching between the paths can be based on simple clip detectors.

We also observe some worst case peaks at 914.5/915/915.5MHz in Path2/3 (see the zoom-in figure for Path 3) despite using the TR modulation. As mentioned in section II-B, this is caused by intermodulation between the signals and interferer. When we model 3rd order intermodulation in the shifted limiter, we see that single tone interferers at $\omega_{sig} \pm \left(0,\ \frac{1}{2}\Delta\omega,\ \Delta\omega,\ \frac{3}{2}\Delta\omega\right)$ produce non-spread intermodulation products at $\Delta\omega$ after the ED. In the measurements we see that only the BER at spacing 0 and ½$\Delta\omega$ is compromised. We hypothesize that the intermodulation products at the other spacings are insufficient to ruin the BER because the magnitude of these products decreases as they get further from the signal frequency, but this should be further investigated.

Figure 16 shows the relationship between the SIR and the interferer symbol rate in Path 3. First of all, an ASK-modulated interferer (50% modulation depth, 920MHz centre frequency) is used to replace the sinusoidal one in the previous setup, and the signal centre frequency is still 915MHz. As we expect, for a narrow ETA_{BW} ($I_{BET} = 2.5$nA), the SIR is deteriorated when the interferer symbol rate is increased. As a comparison, for a wider ETA_{BW} ($I_{BET} = 75$nA), the SIR is effectively improved. Later, a GMSK-modulated interferer (920MHz centre frequency) is adopted. Since the GMSK-modulated interferer has a constant envelope (PDF_{sin}), the related SIR is as good as the one using a sinusoidal interferer (-50dB) even though the ETA_{BW} is very narrow ($I_{BET} = 2.5$nA). Thus because of the TR and SL, our proposed receiver is robust to interferers with constant or slow varying envelopes, so the performance will deteriorate for wideband interferers or multiple widely-spaced strong interferers, which can't meet the restriction in (10). Compared to the ED based [8] (low

power setting) and superheterodyne receivers [2], our in-band SIR at +/- 1/3/5MHz offset is improved by 31/31/31 and 47/28/23dB respectively, although the power consumption is 3 and 2 times higher. Sensitivity is 5dB better than [8] and 36dB worse than [2]. The performance comparison between this work and other state-of-the-arts is summarized in Table I.

V. Conclusion

This paper presents a 175μW 915MHz 10kbps receiver for WSN applications. Transmitted-Reference (TR) modulation is introduced to enhance interference and fading robustness and reach fast synchronization. To further improve the interference robustness, the Shifted Limiter (SL) is proposed. Compared to the RX using TR modulation only (Path 1), the RX using both TR and SL (Path 3) can improve the in-band SIR (at +/- 1MHz offset) by 42dB, while the corresponding power consumption is just increased by 40μW. Interference robustness of the SL is limited by the speed of the Envelope Tracking and Adjusting (ETA) loop, which can track AM interferers up to a bandwidth of approximately 1MHz. Due to its low power, moderate sensitivity and high selectivity, the proposed receiver is suitable for low-power short-range communications in bands with severe narrow-band interference.

Appendix A

The conversion gain of the signal (G_{sig}) and interferer (G_{int}) can be derived by using the Double-Fourier Series (DFS) [20], which are given below:

$$G_{sig} = \frac{1}{2\pi^2 V_{sig}} \iint_{-\pi}^{\pi} f\left(V_{sig}\sin\theta_1 + V_{int}\sin\theta_2\right)\sin\theta_1 \, d\theta_1 d\theta_2 \quad \text{(A.1)}$$

$$G_{int} = \frac{1}{2\pi^2 V_{int}} \iint_{-\pi}^{\pi} f\left(V_{sig}\sin\theta_1 + V_{int}\sin\theta_2\right)\sin\theta_2 \, d\theta_1 d\theta_2 \quad \text{(A.2)}$$

where $\theta_1 = \omega_{sig}t$ and $\theta_2 = \omega_{int}t$. Therefore, the SIR changing ($= G_{sig}/G_{int}$) of the LNA can be estimated if its transfer function is known. What's more, if V_{sig} is close to 0, (A.1) and (A.2) can be approximated as:

$$G_{sig} = \frac{1}{2\pi}\int_{-\pi}^{\pi} f'(V_{int}\sin\theta_2)d\theta_2 \quad (A.3)$$

$$G_{int} = \frac{1}{\pi V_{int}}\int_{-\pi}^{\pi} f(V_{int}\sin\theta_2)\sin\theta_2\, d\theta_2 \quad (A.4)$$

Using x to replace $V_{int}\sin\theta_2$, (A.3) can be modified to

$$G_{sig} = \frac{1}{2\pi}\int_{-V_{int}}^{V_{int}} f'(x)d(\sin^{-1}(\frac{x}{V_{int}})) = \int_{-V_{int}}^{V_{int}} \frac{f'(x)}{\pi\sqrt{V_{int}^2-x^2}}dx \quad (A.5)$$

where $1/(\pi\sqrt{V_{int}^2 - x^2})$ is the Probability Density Function of a sinusoidal wave with amplitude V_{int} (PDF_{sin}). (A.5) shows that the effective signal conversion gain is not only depending on the interferer amplitude, but also the transfer function $f(x)$. Particularly, with the conditions in (7), we assumed $f'(x) = 0$ outside the linear range and $f'(x) = G_S$ within the linear range, thus the integral interval in (A.5) will be changed to the linear range. Finally we have:

$$G_{sig} = G_S \cdot \int_{V_{TH}}^{V_{clip}} PDF_{sin}(x)\, dx \quad (A.6)$$

In the same way, the conversion gain of a differential shifted limiter could be calculated, in which case the integral intervals should be separated into two parts which are from $-V_{clip}$ to $-V_{TH}$ and from V_{TH} to V_{clip}, respectively.

References:

[1]. J. M. Rabaey, J. Ammer, T. Karalar, B. Otis, M. Sheets, and T. Tuan, “Pico Radios for Wireless Sensor Networks: The Next Challenge in Ultra-low Power Design,” in *IEEE ISSCC Dig. Tech. Papers*, pp. 200-201, Feb. 2002

[2] C. Salazar, A. Kaiser, A. Cathelin, and J. Rabaey, “A -97dBm-Sensitivity Interferer-Resilient 2.4GHz Wake-up Receiver Using Dual-IF Multi-N-Path Architecture in 65nm CMOS”, *ISSCC Dig. Tech. Papers*, pp. 1-3, Feb. 2015.

[3] T. Abe, T. Morie, K. Satou, D. Nomasaki, S. Nakamura, Y. Horiuchi, and K. Imamura, “An Ultra-Low-Power 2-step Wake-up Receiver for IEEE 802.15.4g Wireless Sensor Networks,” *IEEE Symp. VLSI Circuits*, pp. 1-2, June 2014.

[4]. N. Pletcher, S. Gambini, and J. Rabaey, “A 65µW, 1.9GHz RF to Digital Baseband Wakeup Receiver for Wireless Sensor Nodes,” in *Proc. IEEE Custom Integrated Circuits Conf.*, pp. 539-542, Sep. 2007

[5]. N. Pletcher, S. Gambini, and J. Rabaey, “A 52µW Wake-up Receiver with -72dBm Sensitivity Using an Uncertain-IF Architecture*”, IEEE J. Solid-State Circuits*, vol.44, no.1, pp. 269-280, Jan. 2009.

[6]. C. Bryant and H. Sjoland, “A 2.45GHz, 50µW Wake-up Receiver Front-end with -88dBm Sensitivity and 250kbps Data Rate,” *European Solid-State Circuits Conf.*, pp. 235-238, Sep. 2014.

[7]. X. Huang, P. Harpe, G. Dolmans, H. de Groot and J. R. Long, “A 780–950 MHz, 64–146 µW Power-Scalable Synchronized-Switching OOK Receiver for Wireless Event-Driven Applications,” *IEEE J. Solid-State Circuits*, vol.49, no.5, pp. 1135-1147, Mar. 2014.

[8]. X. Huang, A. Ba, P. Harpe, G. Dolmans, H. de Groot, and J. R. Long, "A 915MHz, Ultra-low Power 2-tone Transceiver with Enhanced Interference Resilience," *IEEE J. Solid-State Circuits*, vol. 47, no. 12, pp. 3197-3207, Dec. 2012.

[9]. D. Ye, R. van der Zee, and B. Nauta, "An Ultra-Low-Power Receiver Using Transmitted-Reference and Shifted Limiters for In-band Interference Resilience," in *IEEE ISSCC Dig. Tech. Papers*, pp. 438-439, Feb. 2016.

[10]. R. Pickholtz, D. Schilling, and L. Milstein, "Theory of Spread-Spectrum Communications-A Tutorial," *IEEE Trans. on Communications*, vol. 30, no. 5, pp. 855-884, Jun. 1982.

[11]. J. van Sinderen, G. W. de Jong, F. Leong, et al., "Wideband UHF ISM-Band Transceiver Supporting Multichannel Reception and DSSS Modulation," in *Proc. IEEE ISSCC Dig. Tech. Papers*, pp. 453-455, Feb. 2013

[12]. J. J. Spilker, "Some Effects of a Random Channel on Transmitted Reference Signals," *IEEE Trans. on Communication Technology*, vol. 13, no. 3, pp. 377-379, Sep. 1965.

[13]. N. M. Blachman, "Band-pass Nonlinearities," *IEEE Trans. on Information Theory*, vol. 10, no. 2, pp. 162-164, Apr. 1964.

[14]. M. Soer, E. Klumperink, Z. Ru, F. E. van Vliet, and B. Nauta, "A 0.2-to-2.0 GHz 65 nm CMOS Receiver without LNA Achieving 11 dBm IIP3 and 6.5 dB NF," in *IEEE ISSCC Dig. Tech. Papers*, vol. 52, pp. 222–223, Feb. 2009.

[15]. Z. Ru, N. Moseley, E. Klumperink, and B. Nauta, "Digitally Enhanced Software-defined Radio Receiver Robust to Out-of-band Interference," *IEEE J. Solid-State Circuits*, vol. 44, no. 12, pp. 3359–3375, Dec. 2009.

[16]. D. Arnstein, C. Pike, and G. Estep, "On-Board AJ Enhancement Using Adaptive Nonlinear Processing: Practical Aspects of Smart AGC Implementation," *IEEE Military Communications Conf.*, vol. 1, pp. 199-205, Oct. 1992.

[17]. R. G. Meyer, “Low-power Monolithic RF Peak Detector Analysis,” *IEEE J. Solid-State Circuits*, vol. 30, no. 1, pp. 65-67, Jan. 1995.

[18]. E. A. Vittoz, M. G. R. Degrauwe, and S. Bitz, “High-performance Crystal Oscillator Circuits: Theory and Application,” *IEEE J. Solid-State Circuits*, vol. 23, no. 3, pp. 774-783, Jun. 1988.

[19]. P. C. Jain, N. M. Blachman, and P. M. Chapell, “Interference Suppression by Biased Nonlinearities,” IEEE Trans. on Information Theory, vol. 41, no.2, pp. 496-507, Mar. 1995.

[20]. A. Gelb and W. E. Vander Velde, “Multiple Input Describing Functions and Nonlinear System Design,” McGraw-Hill, 1968, pp. 255--305.

List of figures

List of Tables

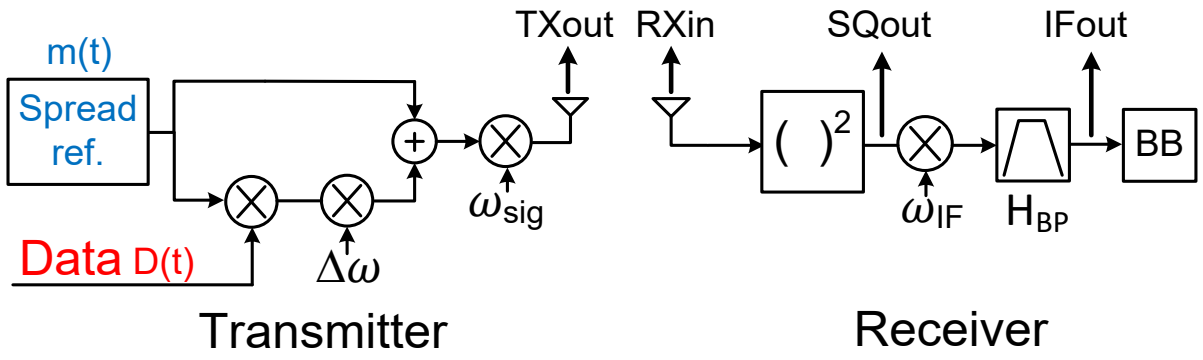

Figure 1. Transceiver architecture of transmitted-reference system.

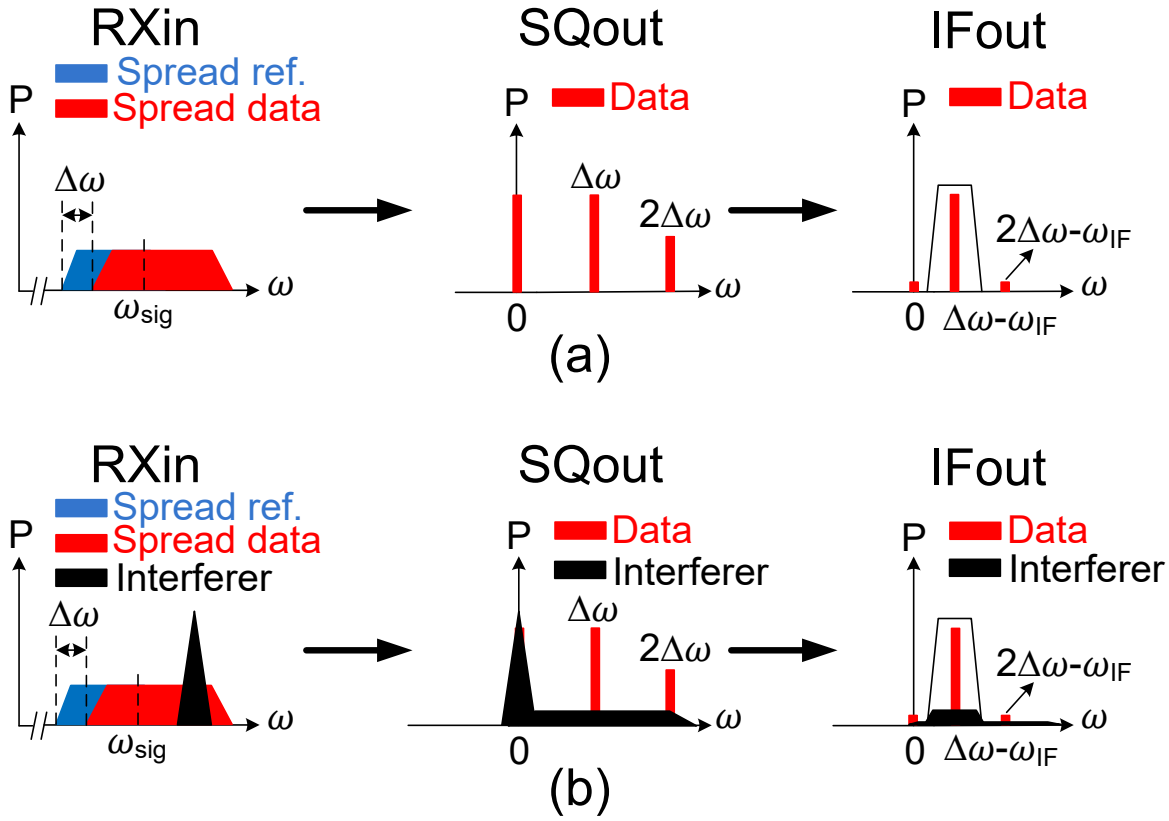

Figure 2. Frequency translation in the TR RX (a) w/o in-band interferer (b) with in-band interferer. The mirror frequencies after each mixing stage are omitted for clearer visualization.

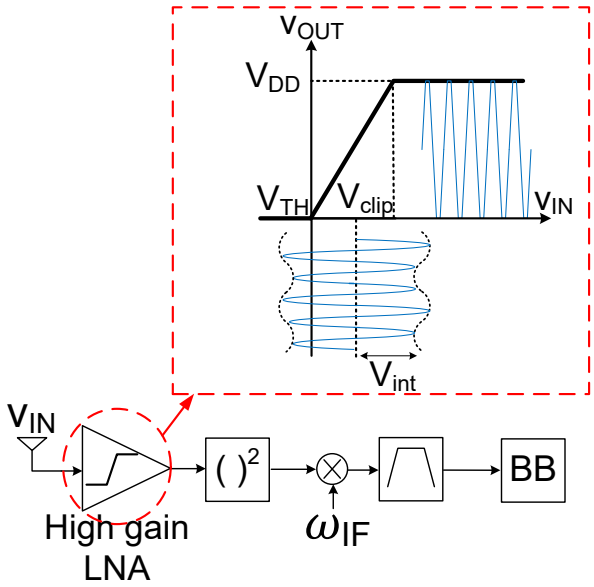

Figure 3. Hard limiting in LNA

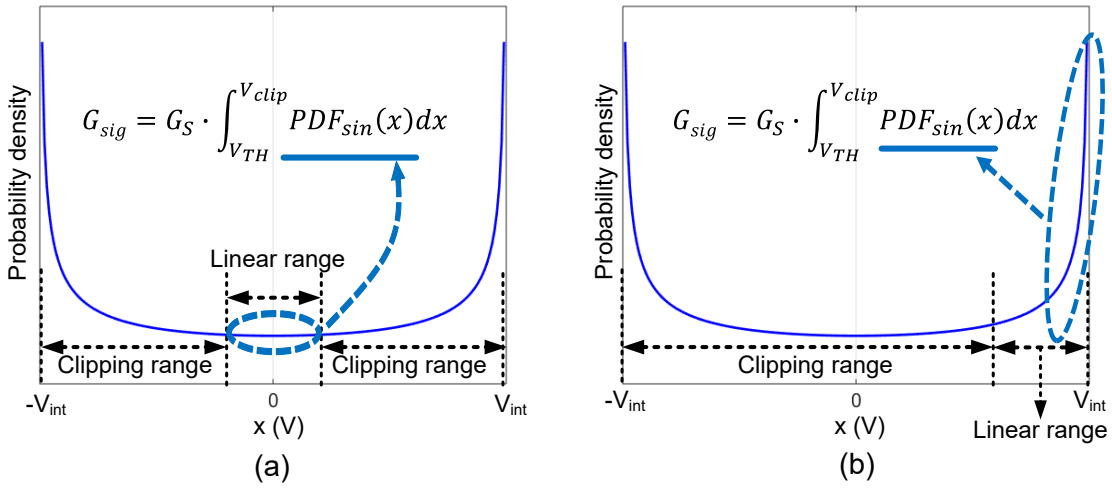

Figure 4. (a) Compression of G_{sig} due to the small part of $PDF_{sin}(x)$ within the linear range.

(b) Compression relaxing of G_{sig} by shifting linear range to have higher $PDF_{sin}(x)$.

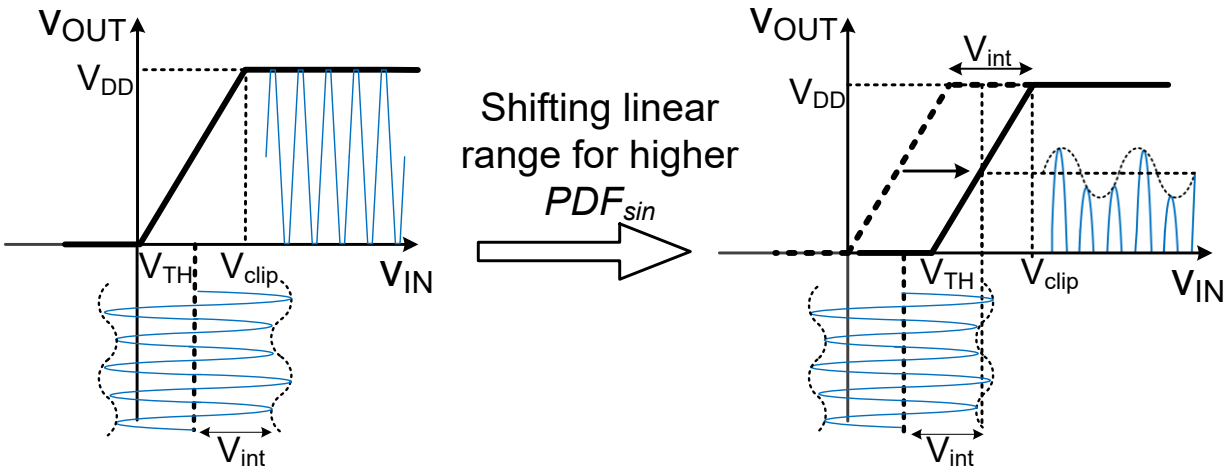

Figure 5. Principle of Shifted Limiter (SL).

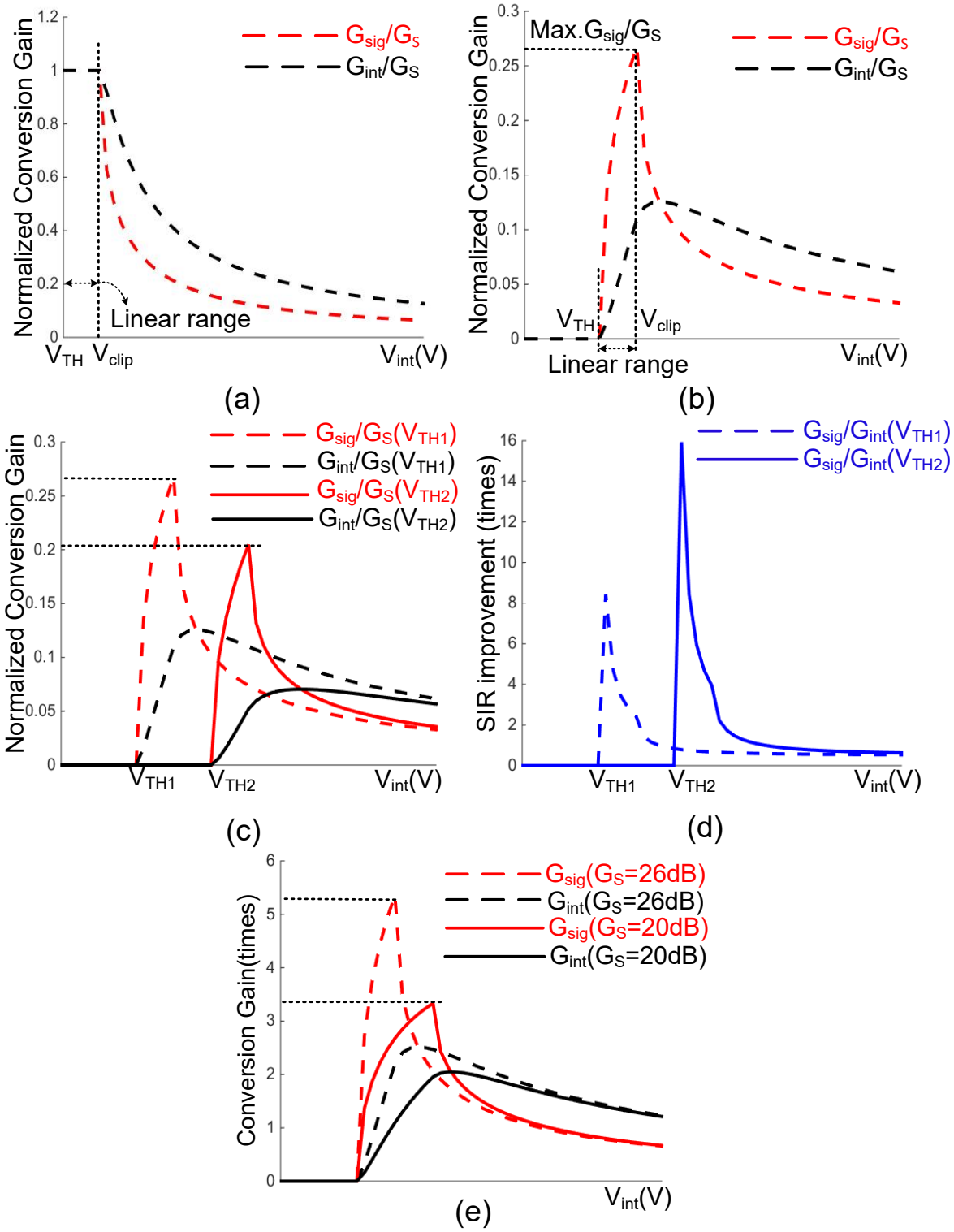

Figure 6. (a) Conversion gain of limiter. (b) Conversion gain of shifted limiter. (c) The SIR improvement (G_{sig}/G_{int}) by changing the threshold voltage ($V_{TH2} = 2V_{TH1}$). (d) SIR improvement for different V_{TH} (e) Conversion gain of shifted limiter for different G_S.

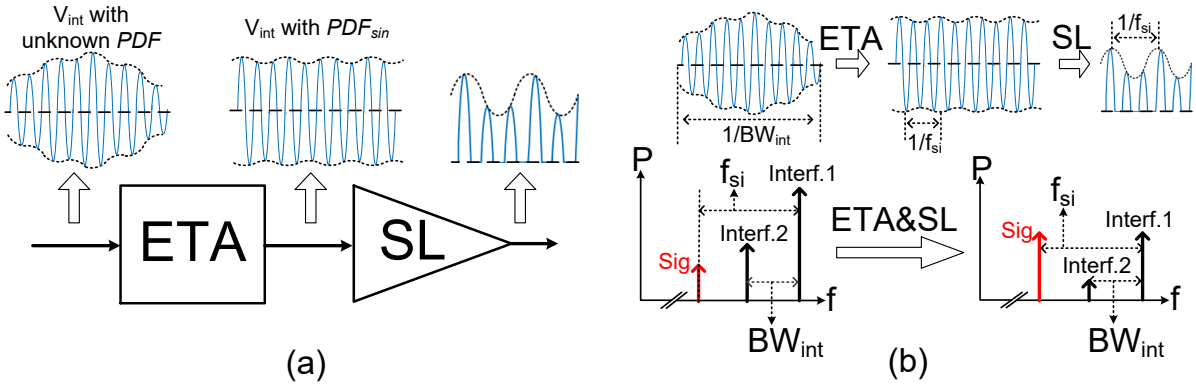

Figure 7. (a) Illustration of Envelope Tracking and Adjusting (ETA) in time domain. (b) Illustration of ETA in frequency domain.

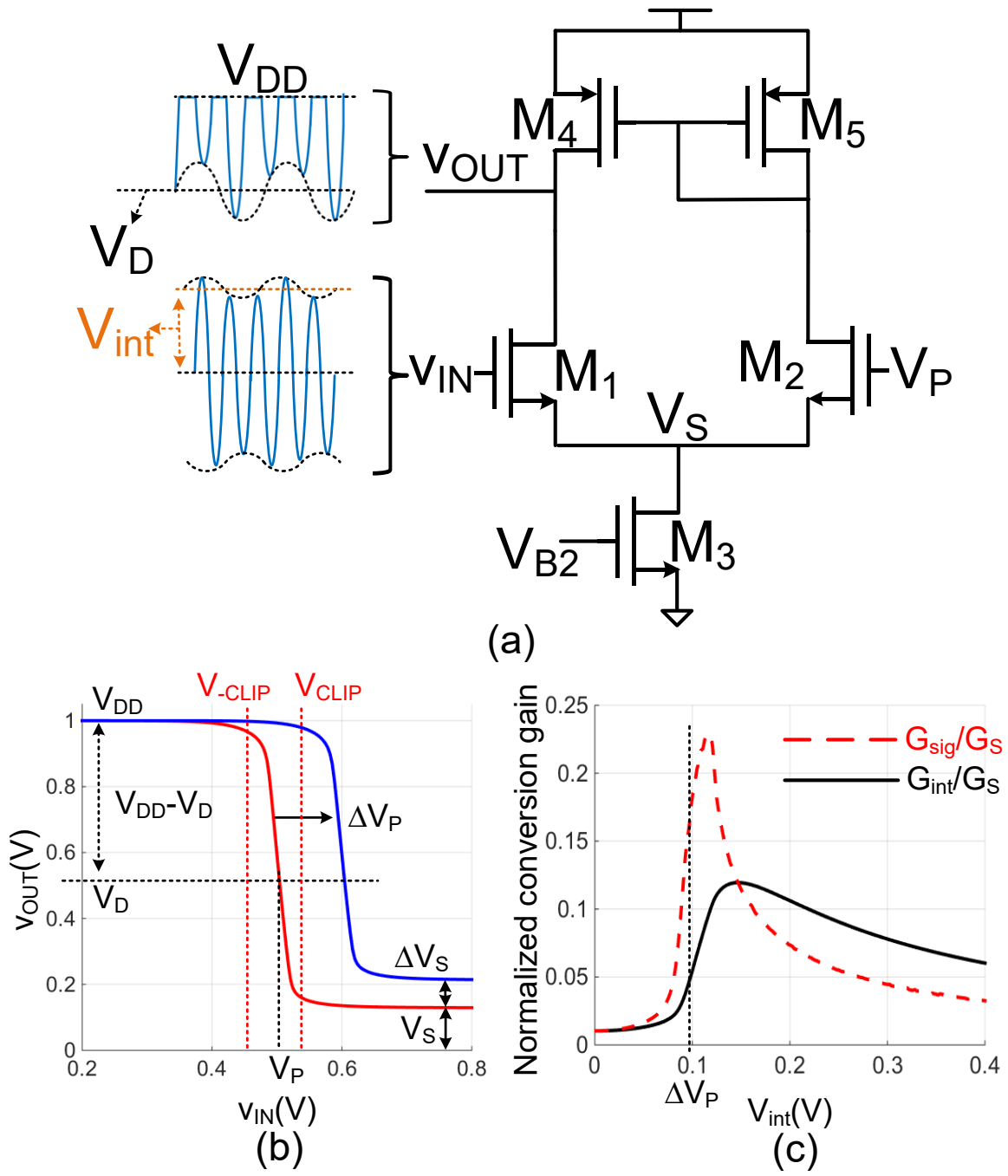

Figure 8. (a) Circuit implementation of SL. (b) Simulated DC characteristics of SL. (c) Simulated conversion gain of signal and interferer for $V_P = 0.1$V.

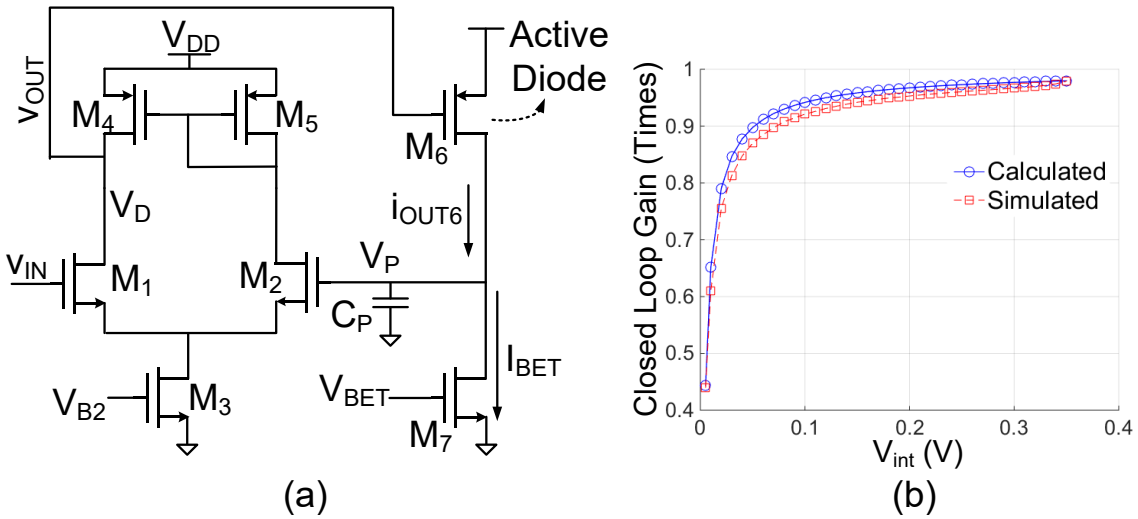

Figure 9. (a) Circuit detail of SL with feedback ETA control. (b) The comparison between the calculated and simulated closed loop gain (G_{CL}) of the proposed SL.

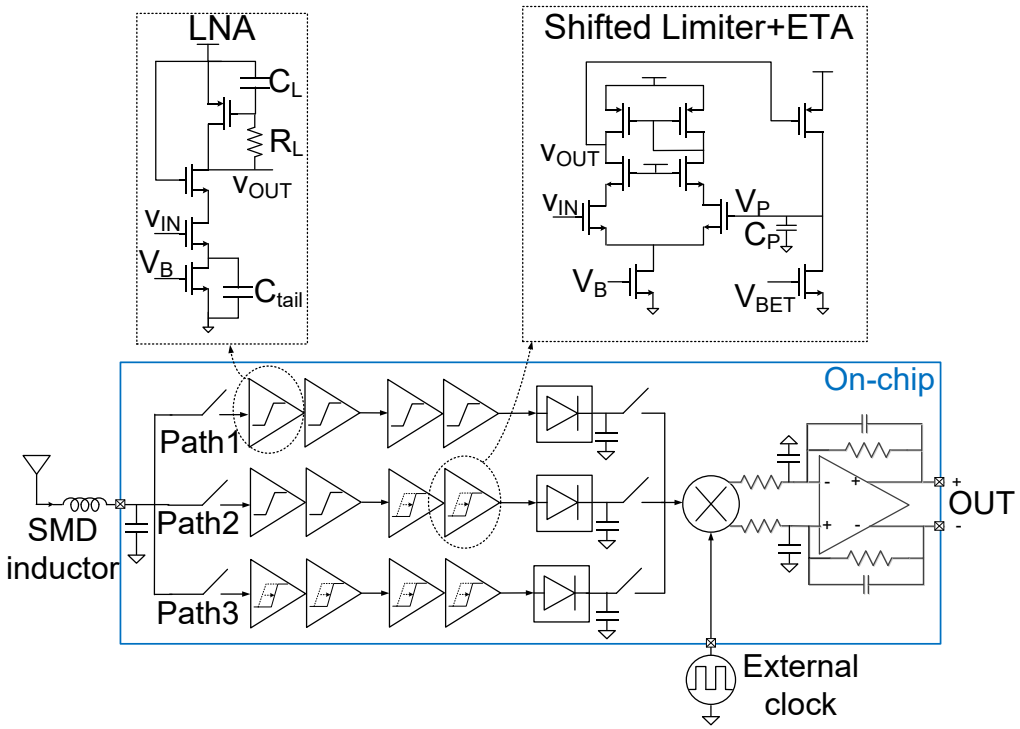

Figure 10. Schematic of the proposed RX.

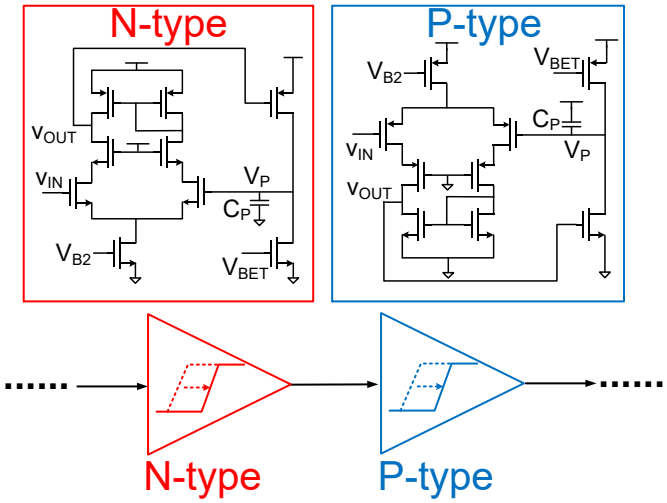

Figure 11. The SL chains composed of different types of SL to further improve the SIR.

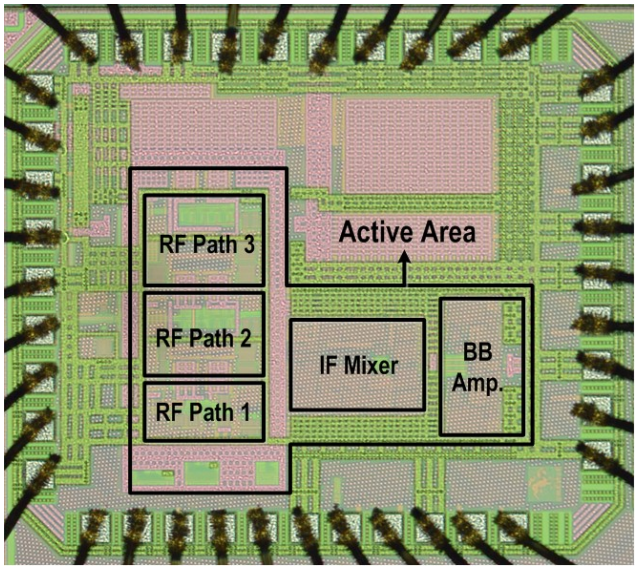

Figure 12. Chip micrograph (1×1mm).

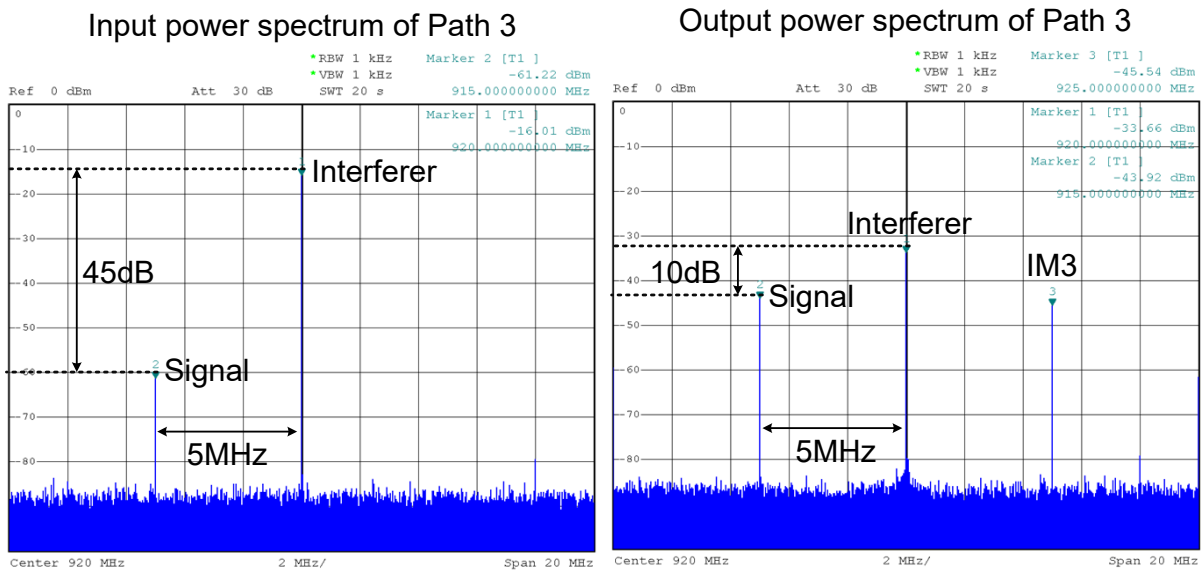

Figure 13. Measured SIR improvement of shifted limiters using two-tone input.

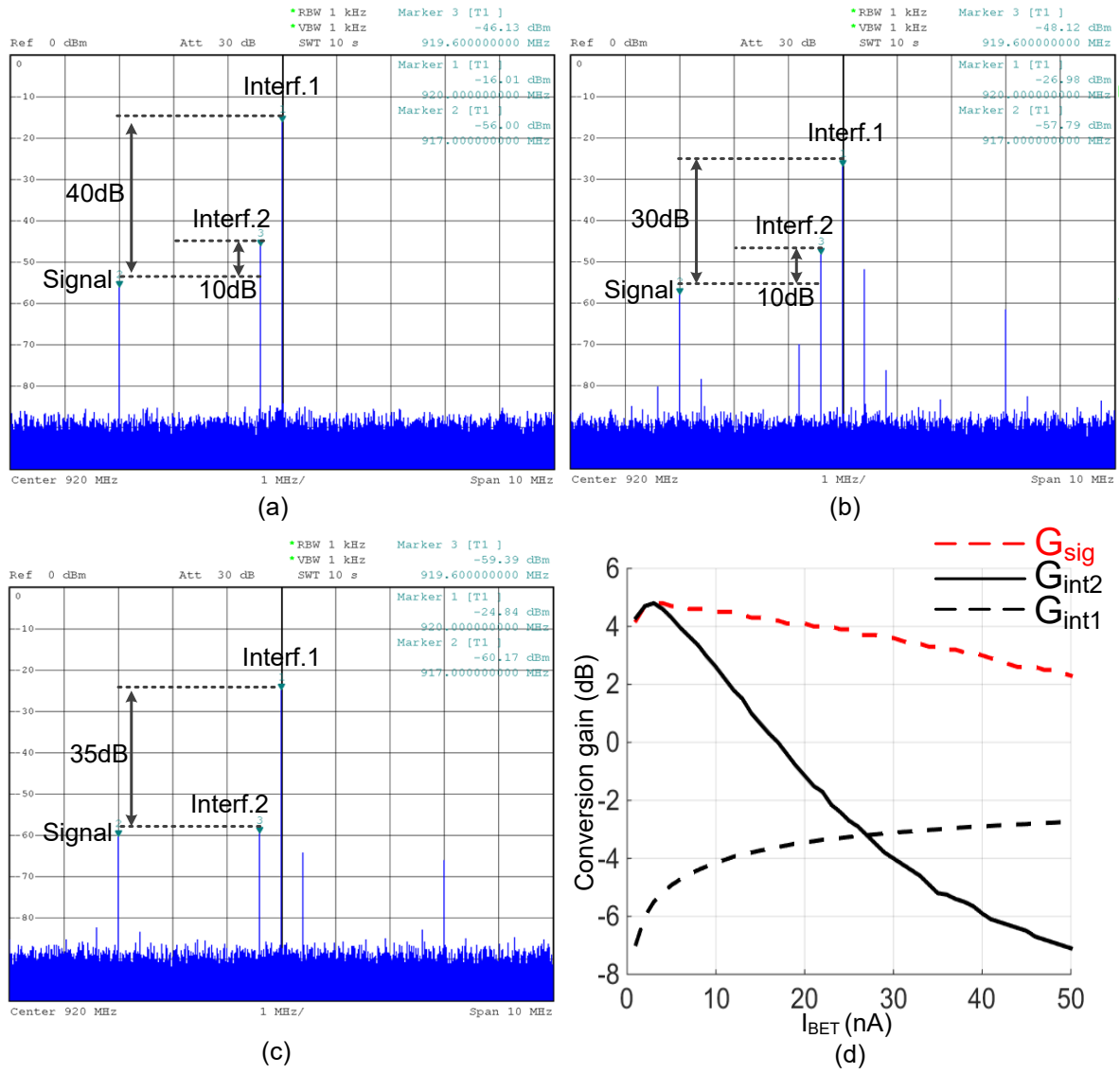

Figure 14. The measured performance of a single SL for AM interferer by adjusting I_{BET}: (a) The input power spectrum of the SL. (b) The output power spectrum of the SL (I_{BET} = 5nA). (c) The output power spectrum of the SL (I_{BET} = 50nA). (d) The relationship between G_{sig}, G_{int1}, G_{int2} and I_{BET}.

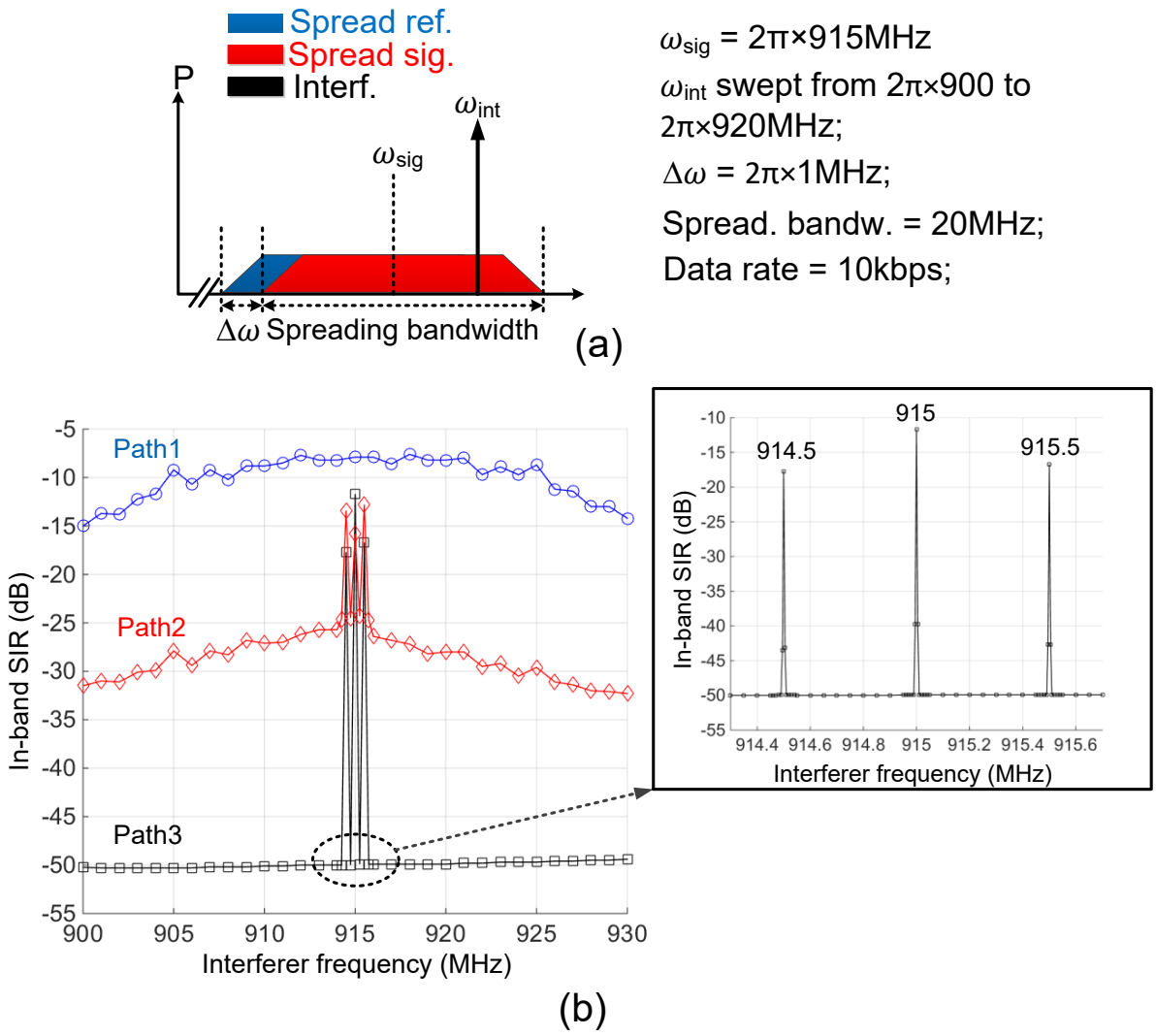

Figure 15. (a) Input signal for the SIR measurement of the proposed receiver. (b) Measured SIR of the proposed receiver for different RF paths.

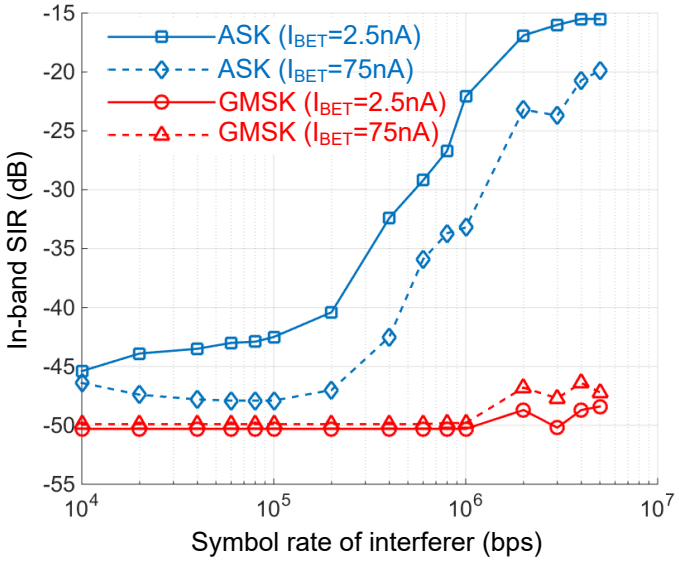

Figure 16. Measured relationship between the in-band SIR and interferer symbol rate in Path 3 for I_{BET} = 2.5 and 75nA respectively.

ULP RX	[2]		[3]		[5]	[8]		This work		
Frequency (MHz)	2400		924		2000	915		915		
Techniques for Interf. robustness	Dual-IF+N-Path		Low-IF+Digital bit length detection		FBAR filter	SAW filter+Two-tones		Transmitted-Reference+Shifted Limiter		
			EDRX	ADRX				Path3	Path2	Path1
Instant. Power (μW)	99		44	1300	52	63	121	175	150	135
Sensitivity (dBm)	-92	-97	-87	-87	-72	-56	-83	-61	-70	-76
In-band SIR (dB)[1] @+/- 1MHz @+/- 3MHz @+/- 5MHz	 N/A N/A N/A	 -3 -22 -27	 N/A N/A N/A	 -60/0[2] -5/-38[3] N/A	 N/A N/A N/A	 -19 -19 -19	 -10.5 -10.5 -10.5	 -50 -50 -50	 -26 -26 -27	 -8 -8 -8
Data rate (kbps)	50	10	1	50	100	10		10		

(1): Worst value of positive/negative offsets from the centre frequency

(2): High SIR ratio @+1MHz since interferer frequency = LO frequency.

(3): Very a-symmetric SIR

Table I. Performance comparison table of state-of-the-art.